Submitted to the 29th International Conference on High-Energy Physics ICHEP98,
Vancouver, Canada, July 1998

Measurements of the diffractive structure function $F_2^{D(3)}$ at low and high Q^2 at HERA

H1 Collaboration

Abstract

Measurements of the diffractive structure function $F_2^{D(3)}(x_{I\!P}, \beta, Q^2)$, describing the process $ep \to eXY$, are presented in the two kinematic regions $0.4 \leq Q^2 \leq 5$, GeV^2, $0.001 \leq \beta \leq 0.65$, and $200 \leq \beta \leq 800\ \mathrm{GeV}^2$, $0.4 \leq \beta \leq 0.9$, both with $x_{I\!P} < 0.05$, $M_Y < 1.6$ GeV and $|t| < 1.0\ \mathrm{GeV}^2$. Together with published measurements at intermediate Q^2, the data are compared with models based on QCD and Regge phenomenology. The $x_{I\!P}$ dependence of the data can be described in a model based on the exchange of a dominant diffractive trajectory with additional sub-leading reggeon contributions. The diffractive trajectory is found to have an intercept larger than that describing soft hadronic data and consistent with that determined using previously published H1 measurements at intermediate Q^2 alone. The high Q^2 data are well described by a QCD fit to the published data in which parton distributions, evolving according to the DGLAP equations, are assigned to the leading and sub-leading exchanges. The data are also parameterised using a QCD motivated model based on the exchange of two gluons from the proton. In this model, the higher twist contribution to $F_2^{D(3)}$ at large β is found to be important at low Q^2. The data are also compared with models based on BFKL dynamics.

Abstract: 571
Parallel sessions: 5, 4
Plenary sessions: 7, 6

1 Introduction

In this paper, we report measurements of the diffractive structure function $F_2^{D(3)}(\beta, Q^2, x_{I\!P})$ based on deep-inelastic scattering (DIS) data taken between 1995 and 1997 by the H1 collaboration. The $F_2^{D(3)}$ measurement describes the process $ep \to eXY$ as illustrated in figure 1. As in our previous analysis of 1994 data [1], the two distinct hadronic systems X and Y are separated by the largest interval in rapidity between final state hadrons. The system Y is closest to the direction of the outgoing proton beam.

The kinematics of the process can be described by the invariant masses M_X and M_Y of the systems X and Y, and the Lorentz scalars

$$x = \frac{-q^2}{2P \cdot q} \qquad y = \frac{P \cdot q}{P \cdot k} \qquad Q^2 = -q^2 \qquad t = (P - P_Y)^2 \, , \tag{1}$$

where P and k are the 4-momenta of the incident proton and electron respectively, P_Y is the 4-momentum of subsystem Y and q is the 4-momentum of the exchanged virtual photon coupling to the electron. The measurements presented here are corrected to the region $M_Y < 1.6$ GeV and $|t| < 1.0$ GeV^2. The following variables are also defined:

$$\beta = \frac{-q^2}{2q \cdot (P - P_Y)} = \frac{Q^2}{Q^2 + M_X^2 - t} \qquad x_{I\!P} = \frac{q \cdot (P - P_Y)}{q \cdot P} = \frac{Q^2 + M_X^2 - t}{Q^2 + W^2 - M_P^2} = \frac{x}{\beta} \, , \tag{2}$$

where $W^2 = (q + P)^2$ is the center of mass energy squared of the virtual photon-proton system, M_P the proton mass and x is the Bjorken scaling variable.

During the 1994/95 HERA shutdown, the backward region of the H1 detector [2] (the direction of the outgoing electron beam) was upgraded, allowing an extension of $F_2^{D(3)}$ measurements to lower Q^2 and β values compared to 1994. Using data taken during a period when the interaction vertex was shifted by 70 cm in the proton beam direction, the accessible kinematic range is extended still further. The minimum value of Q^2 at which F_2^D is measured is thus reduced by a factor 10 and the minimum β by a factor 40 compared to the previous measurement [1].

The good running of the HERA machine in recent years has enabled a large increase in the integrated luminosity recorded by H1. One impact of this increase in statistics is the extension of the accessible kinematic range to higher values of Q^2. A measurement of $F_2^{D(3)}$ for $200 \leq Q^2 \leq 800$ GeV^2 is presented in this paper, based on positron-proton scattering data collected in the years 1995-1997. This data sample represents an increase in statistics by a factor of around 15 compared to previous H1 $F_2^{D(3)}$ measurements [1].

2 The H1 detector

The H1 detector [2] is a multi-purpose apparatus built to investigate the final state of high energy electron-proton interactions. A brief account is given here of the components that are most important to the F_2^D measurement. In the coordinate convention used by the experiment, the "forward", positive z, direction corresponds to that of the outgoing proton beam, with polar angles θ measured with respect to this direction and pseudorapidities defined as $\eta = -\ln(\tan\theta/2)$.

In the low Q^2 analysis, the energy of the final state electron is measured in the lead / scintillating fiber calorimeter SPACAL [3], which replaced the previous electromagnetic calorimeter (BEMC). The calibration of the SPACAL is described in [4]. Its angular acceptance is $153 < \theta < 177.8°$ for collisions at nominal vertex position and extends to $178.5°$ when the interaction point is shifted by 70 cm in the proton direction. The electromagnetic part of the SPACAL includes a veto layer immediately around the beam-pipe (inner and outer radii of 5.7 cm and 6.5 cm respectively) which is used to reject electrons for which the shower is not fully contained in the detector. The time resolution of the SPACAL calorimeter is better than 1 ns, which allows the rejection of background from beam interactions with the beam-pipe walls or with gas particles outside the H1 detector.

An eight layer drift chamber (BDC) [5] is located in front of the SPACAL calorimeter, providing an angular coverage of $151 \leq \theta \leq 178.3°$ under the shifted vertex conditions. The BDC replaces the backward proportional chamber used in the 1994 analysis. It is used to identify and measure the polar angle of electrons with the additional use of a reconstructed vertex position in the z coordinate.

In the high Q^2 analysis, the final state electron is detected and measured in the highly segmented liquid argon (LAr) calorimeter, which covers the angular region $3 \leq \theta \leq 155°$. The depth of the electromagnetic part of the LAr varies between 20 and 30 radiation lengths. Its electromagnetic energy scale is known to better than 1%.

The hadronic final state system X is measured with the combined use of the hadronic part of the liquid argon calorimeter, the hadronic part of the SPACAL calorimeter and the central tracking components of the detector. The central tracking system covers the pseudorapidity range $-1.5 < \eta < 1.5$ with the vertex in its nominal position. A uniform 1.15 T magnetic field created by a superconducting solenoid surrounds both the tracking system and the liquid argon calorimeter.

Luminosity is determined from the measured rate of the Bethe Heitler process $ep \rightarrow ep\gamma$, detecting the electron and the photon in crystal calorimeters located respectively at z=-33 m and z=-103 m. The luminosity of the low Q^2 sample is known with an accuracy of 2.6% [6]. The luminosity of the high Q^2 sample is known to 1.8%.

Events with large forward rapidity gaps separating the systems X and Y are selected with the use of several detectors overlapping in their pseudorapidity coverage: the forward part of the liquid argon calorimeter, the copper-silicon PLUG calorimeter, the forward muon detector (FMD) and the proton remnant tagger (PRT). These detectors are sensitive to particles emitted in the pseudorapidity range $3.5 < \eta < 7.5$ [1].

3 Event selection and kinematic reconstruction

3.1 Deep-inelastic selection

The data sample used for the low Q^2 measurement corresponds to an integrated luminosity of 122 nb^{-1}. Events were triggered by requiring a local energy deposit (cluster) in the SPACAL calorimeter with an energy greater than about 5 GeV, occurring at a time compatible with the expectation for an ep interaction in the vertex region. The trigger efficiency is about 98% for electrons with an energy greater than 7 GeV. The timing requirement induces losses of about 1%.

To obtain a sample of low Q^2 DIS events, it was required that the most energetic electromagnetic cluster in the SPACAL calorimeter, taken as the electron candidate, has an energy greater than 7 GeV with a signal within a time window of 4 ns width around the expected arrival time. The cluster radius of the electron candidate was required to be less than 3.5 cm, characteristic of an electromagnetic shower. A track segment was required in the BDC, matching the cluster in the SPACAL calorimeter within 2.5 cm. In order to avoid losses of energy into the beampipe, events with more than 1 GeV of energy deposited in the veto layer of the SPACAL calorimeter were rejected and the radial distance between the beam line and the point at which the BDC track intersects the surface of the SPACAL was required to be larger than 9 cm.

The high Q^2 sample is based on all available data taken in 1995-1997, amounting to an integrated luminosity of $31.7\ \mathrm{pb}^{-1}$. High Q^2 DIS events were triggered on the basis of a "tower" of electromagnetic energy in the LAr, pointing towards the event vertex. This trigger condition has an efficiency in excess of 99.5% for electrons with energy greater than $11\ \mathrm{GeV}$.

High Q^2 events were selected by identifying the scattered positron with the requirement of a compact, electromagnetic, high energy deposit in the liquid argon calorimeter, together with an associated track in the tracking detectors pointing to the interaction point. QED Compton events ($ep \to ep\gamma$) were rejected by requiring at least 2 tracks in events where greater than 90% of the energy of the final state, excluding the electron, was reconstructed in the electromagnetic section the the liquid argon calorimeter.

Cosmic and beam induced backgrounds were reduced to negligible levels in both samples by requiring a vertex reconstructed within 35 cm of the nominal interaction point and that the timing of the signals from the tracking detector be within the interval expected for ep collisions. Radiative events and photoproduction events in which a hadron is misidentified as the scattered electron were suppressed by requiring $35 < \Sigma(E - Pz) < 75$ GeV, where the sum extends over all final state hadrons and the scattered electron.

The efficiency of the DIS selection is better than 85% for a large part of the kinematic domain.

3.2 Rapidity gap selection

To select a sample of events where colourless exchange dominates, it is required that no signal be recorded above noise levels in a number of forward components of H1. The following conditions must be satisfied:

- no cluster with energy greater than 400 MeV in the forward part of the liquid argon calorimeter ($\eta > 3.2$).
- at most one hit pair in the first three layers of the forward muon detector.
- no signal in the proton remnant tagger.
- no cluster with energy greater than 2.5 GeV in the PLUG calorimeter.

These selection criteria imply that the systems X and Y are well separated and that X is fully contained in the main part of the H1 detector. The system Y goes unobserved into the beam pipe, implying that $M_Y \lesssim 1.6$ GeV, and $|t| \lesssim 1$ GeV^2.

3.3 Kinematic reconstruction

Two methods are used in the reconstruction of the kinematic variables x, y and Q^2. In the electron method, the relationships

$$Q_e^2 = 4E_e' E_e \cos^2 \frac{\theta_e}{2} \qquad\qquad y_e = 1 - \frac{E_e'}{E_e} \sin^2 \frac{\theta_e}{2} \,, \tag{3}$$

are used, where E_e is the electron beam energy and E_e' and θ_e are respectively the energy and polar angle of the scattered electron. The Σ method [7] uses information from both the scattered electron and the hadronic final state measurement:

$$Q_\Sigma^2 = \frac{E_e' \sin^2 \theta_e}{1 - y_\Sigma} \qquad\qquad y_\Sigma = \frac{\Sigma}{\Sigma + E_e'(1 - \cos\theta_e)} \,, \tag{4}$$

where $\Sigma = \Sigma(E - P_z)$ is the sum over all hadronic final state particles of the difference between their energy and longitudinal momentum. The Σ method is less sensitive to radiative corrections, though the electron method gives the best resolution in the low y region.

For the low Q^2 measurement, the electron method is used for data points with $y \geq 0.2$ and the Σ method is used for $y < 0.2$. The expression $x = Q^2/sy$ is used for both methods, where s is the ep center of mass energy squared. In the region of overlap $0.1 \lesssim y \lesssim 0.3$, the agreement between the data points measured with the Σ and the electron methods is well within the statistical uncertainties. At high Q^2, the $e\Sigma$ method [7] is used to achieve the best resolution. Q^2 is reconstructed using the electron method, x is reconstructed using the Σ method and y is calculated as $y_{e\Sigma} = Q_e^2/sx_\Sigma$.

The mass M_X is used to compute $x_{I\!P}$ and β according to equation (2). M_X is reconstructed using procedures that combine information from the calorimeters with vertex fitted tracks without double counting [8, 9].

4 Cross section and structure function measurement

The large rapidity gap samples defined in the previous section are used to measure the differential cross section $\mathrm{d}^3\sigma/\mathrm{d}Q^2\mathrm{d}\beta\mathrm{d}x$ for the process $ep \to eXY$. The intervals in Q^2, β and x are chosen such that they are always larger than the resolution. The results are corrected to the region $M_Y < 1.6$ GeV, and $|t| \leq 1$ GeV^2.

Acceptance losses due to the cuts are evaluated bin by bin directly from the data or by using a Monte Carlo simulation of the detectors. Corrections for migrations in the kinematic variables due to the finite resolution are determined using Monte Carlo programs with a full simulation of the H1 detector in its configuration for each period of data taking. The details of the simulations used are given in [1]. Diffractive DIS is modelled using the RAPGAP Monte Carlo model [10]. RAPGAP is based on the exchange of a partonic pomeron or meson with leading order QCD matrix elements describing the deep-inelastic scattering of the electron from the colourless exchange. The pomeron and meson flux and parton distributions are determined from previous data [1]. Higher order QCD corrections are provided by the colour dipole model as implemented in ARIADNE [11]. At low M_X, where the resonances ρ, ω, ϕ become important, the additional Monte Carlo model DIFFVM [12] is used. Migrations into the sample from the regions $x_{\mathbb{P}} > 0.1$ and $M_Y > 5$ GeV are studied with the additional use of the DJANGO Monte Carlo simulation [13] of inclusive deep-inelastic ep scattering.

Background from ep interactions arises from photoproduction events ($Q^2 \sim 0$) in which the electron signal is faked by a hadron detected in the SPACAL calorimeter. For about 10% of these events, the scattered electron is detected in the electron tagger of the luminosity system. The photoproduction background, estimated using the PHOJET Monte Carlo model [14] normalised to tagged photoproduction events (see [4]), is concentrated at low x and Q^2 and never exceeds 15%. Residual QED-Compton background is smaller than 2% for all data points and is subtracted statistically bin-by-bin. Other backgrounds, such as that due to interactions of the beams with gas particles in the beam pipe or with beam line elements upstream of the H1 detector, are found to be negligible.

The correction required for migrations about the limit of the measurement $M_Y < 1.6$ GeV is determined using a DIFFVM simulation of vector meson production containing processes both where the proton dissociates and where it remains intact. Due to differences in the efficiencies of the forward detectors, this correction changes from $0 \pm 5\%$ in 1995 to $6 \pm 5\%$ in 1997. Fluctuations in the level of noise in the forward detector components result in some events being wrongly rejected from the samples. The losses due to noise are determined using randomly triggered events. An overall correction of 12.8±3.0 % is applied to the low Q^2 measurement. For the high Q^2 measurement the correction is $8.3 \pm 6.0\%$. Radiative corrections are calculated bin by bin using the HERACLES program [15] interfaced to RAPGAP. They are smaller than 20% for all measured data points. Bin centre corrections are performed based on the parameterisations of the data described in sections 5.1 and 5.2.

The structure function $F_2^{D(3)}$ is calculated from the differential cross section according to the formula

$$F_2^{D(3)}(Q^2, \beta, x_{\mathbb{P}}) = \frac{\beta^2 Q^4}{4\pi\alpha_{em}^2} \frac{1}{(1 - y - \frac{y^2}{2})} \frac{\mathrm{d}^3\sigma_{ep\to eXY}}{\mathrm{d}Q^2\,\mathrm{d}\beta\,\mathrm{d}x}\,, \tag{5}$$

taking the ratio R of the longitudinal to the transverse cross sections to be 0.

Systematic errors from the following sources are considered:

- The uncertainties in the electromagnetic energy scales of the SPACAL and LAr. For the SPACAL, this uncertainty varies linearly from 1.5% at large energies to 3% at $E'_e = 7$ GeV. For the LAr, the electromagnetic energy scale is known to 1%.
- The uncertainty in the electron angle θ_e. This is 1 mrad for both data samples.
- The uncertainty in the hadronic energy scale, which is 4% for the liquid argon calorimeter and 10% for the SPACAL. The uncertainty in the energy fraction carried by the tracks is known to 3% accuracy.
- The errors on the determination of detector efficiencies from data. For the low Q^2 analysis, these are typically around 10%. The corresponding uncertainty in the high Q^2 sample is 2%.
- The uncertainty due to photoproduction and QED-Compton backgrounds, which are taken to be 30% of the applied correction.

- There is a 5% systematic uncertainty in the correction to the region $M_Y < 1.6$ GeV, evaluated in the manner described in [8].

- The uncertainties in the forward detector noise contributions lead to systematic errors of 3% for the low Q^2 data and 6% at large Q^2.

- The systematic error in the luminosity determination is 2.6 % for the low Q^2 data and 1.8% for the high Q^2 sample.

- A systematic error of 50% is ascribed to the fraction of events migrating into the sample from the unmeasured region $x_{I\!P} > 0.1$.

- The uncertainty in the input pomeron structure function and flux in the RAPGAP simulation is estimated by reweighting the generated events by factors $x_{I\!P}^{\pm 0.2}$, $e^{\pm 2t}$ and $((1/g - g)\beta + g)$ with $g = 0.5$ or 2.

- The uncertainties due to higher order radiative corrections and the absence of soft photon exponentiation in the HERACLES program lead to a 2% global error.

- The uncertainty in the description of hadronisation, estimated from the differences in the correction factors obtained with the RAPGAP Monte Carlo model when fragmentation is simulated with the colour dipole or parton showering models.

To check that there are no uncontrolled systematic effects in the data, the measurements are repeated with several variations in the kinematic reconstruction and forward pseudorapidity gap selection methods. In all cases, the measured data points remain stable at the level of the statistical errors.

The low Q^2 structure function, measured in the region $0.8 \leq Q^2 \leq 5$ GeV^2, $0.001 \leq \beta \leq 0.65$, and $0.00005 \leq x_{I\!P} \leq 0.05$ is presented in the form of $x_{I\!P} \cdot F_2^{D(3)}$ in figure 2. The statistical errors are shown added in quadrature with those systematic errors that vary from bin to bin. Overall normalisation uncertainties are quoted separately. The low Q^2 measurement displays similar features to the previous measurement at higher Q^2 [1] with $x_{I\!P} F_2^D$ either falling or flat as $x_{I\!P}$ increases at fixed β and Q^2 throughout most of the kinematic range. The high Q^2 data are shown in figure 3. Due to the kinematic constraints imposed by the large Q^2 values, the measurements are restricted to $\beta \geq 0.4$ and relatively large $x_{I\!P}$. At the largest values of β accessed, $x_{I\!P} \cdot F_2^{D(3)}$ is once again flat or falling as a function of $x_{I\!P}$. At lower β, however, $x_{I\!P} \cdot F_2^{D(3)}$ rises with $x_{I\!P}$.

5 Comparisons with models

5.1 Regge parameterisation of the data

The low Q^2 diffractive structure function measurements shown in figure 2 are investigated in the framework of the Regge phenomenological model developed in section 5 of [1]. In this model, the $x_{I\!P}$ dependence at fixed β and Q^2 is parameterised using Regge phenomenology.

First, the 1995 low Q^2 data alone are subjected to a fit in which a single factorisable trajectory ($I\!P$) is exchanged such that:

$$F_2^{D(3)}(Q^2, \beta, x_{I\!P}) = f_{I\!P/p}(x_{I\!P}) F_2^{I\!P}(Q^2, \beta) \; . \tag{6}$$

In this parameterisation, $F_2^{I\!P}$ can be interpreted as a structure function for the pomeron [16]. The value of $F_2^{I\!P}$ is treated as a free parameter at each point in β and Q^2. The pomeron flux takes a Regge form with a linear trajectory $\alpha_{I\!P}(t) = \alpha_{I\!P}(0) + \alpha'_{I\!P}t$, such that

$$f_{I\!P/p}(x_{I\!P}) = \int_{t_{cut}}^{t_{min}} \frac{e^{B_{I\!P}t}}{x_{I\!P}^{2\alpha_{I\!P}(t)-1}} \mathrm{d}t \,, \tag{7}$$

where $|t_{min}|$ is the minimum kinematically allowed value of $|t|$ and $t_{cut} = -1$ GeV^2 is the limit of the measurement . The value of $\alpha_{I\!P}(0)$ is a further free parameter and $B_{I\!P}$ and $\alpha'_{I\!P}$ are taken from hadron-hadron data [1]. In order to avoid the region that may be most strongly affected by a non-zero value of R, only data with $y < 0.6$ are included in the fit. The fit with a single trajectory does not give a good description of the data ($\chi^2/\mathrm{dof} = 65.5/19$ with statistical errors only). This confirms the observations at both higher Q^2 [1] and at $Q^2 = 0$ [8] that secondary trajectories in addition to the pomeron are required to describe diffractive ep data.

Combining the 1994 and the low Q^2 1995 data, a much better fit is obtained when both a leading ($I\!P$) and a sub-leading ($I\!R$) trajectory are considered, such that

$$F_2^{D(3)}(Q^2, \beta, x_{I\!P}) = f_{I\!P/p}(x_{I\!P}) F_2^{I\!P}(Q^2, \beta) + f_{I\!R/p}(x_{I\!P}) F_2^{I\!R}(Q^2, \beta) \,. \tag{8}$$

The flux factor for the secondary trajectory takes the same form as equation (7), with $B_{I\!R}$, and $\alpha'_{I\!R}$ again taken from hadron-hadron data [1]. This fit yields $\chi^2/\mathrm{dof} = 176.3/152$. The resulting value of $\alpha_{I\!P}(0)$ is in agreement with that obtained from the 1994 data alone ($\alpha_{I\!P}(0) = 1.203 \pm 0.020\ (\mathrm{stat.}) \pm 0.013\ (\mathrm{syst.})^{+0.030}_{-0.035}\ (\mathrm{model})$ [1]) and is significantly larger than values extracted from soft hadronic data ($\alpha_{I\!P}(0) \sim 1.08$). The result of this fit is compared with the data in figure 2. The quality of the fit is similar if interference between the two trajectories is introduced.

The Regge fits have not been performed directly on the new high Q^2 data. However, the rise in $x_{I\!P} \cdot F_2^{D(3)}$ for $\beta \leq 0.65$ is indicative of a large contribution from the sub-leading exchange, as would be expected at the comparatively large values of $x_{I\!P}$ accessed. At $\beta = 0.9$, where meson structure functions are small, $x_{I\!P} \cdot F_2^{D(3)}$ is flat or falling with increasing $x_{I\!P}$, as expected for the dominant exchange of a diffractive trajectory with $\alpha_{I\!P}(0) > 1$.

5.2 Model of $F_2^{D(3)}$ with a DGLAP Evolving Partonic Pomeron.

In Figure 4, the Q^2 and β dependences of the 1994 and low Q^2 1995 measurements of $F_2^{D(3)}(Q^2, \beta, x_{I\!P})$ are shown at a fixed small value of $x_{I\!P}$ ($x_{I\!P} = 0.005$), for which sub-leading exchange contributions are small. The Regge fit with two trajectories described in section 5.1 is used to interpolate and extrapolate the data to this $x_{I\!P}$ value. The previously reported scaling violations with positive $\mathrm{d}F_2^{D(3)}/\mathrm{d}\log Q^2$ persist to comparatively high values of β for the new data, indicating a large contribution from gluons in the exchange. In the large β, low Q^2 region, additional structures are observed. These are presumably related to higher twist contributions, in particular, the resonant production of vector mesons.

In section 6 of [1], a Regge model of the 1994 data, similar to that described in section 5.1, was extended by modelling the β and Q^2 dependence of $F_2^{I\!P}$ in terms of parton dynamics. Quark flavour singlet and gluon distributions were ascribed to the pomeron, parameterised using the first three terms of Chebychev polynomials at the starting scale $Q_0^2 = 3\ \mathrm{GeV}^2$. The structure function of the secondary reggeon was taken from a parameterisation for the pion [17], with a free global normalisation determined by the data. The combined parton distributions were then evolved to larger Q^2 using the next-to-leading order (NLO) DGLAP equations [18]. The trajectory intercepts were fixed to $\alpha_{I\!P} = 1.20$ and $\alpha_{I\!R} = 0.57$ [1] according to the results of the pure Regge phenomenological fits. Only data points with $Q^2 \geq 3$ GeV^2, $\beta \leq 0.65$, $M_X > 2$ GeV and $y \leq 0.45$ were included in the fit in order to avoid large higher twist effects and the region that may be most strongly affected by a non zero value of R. The best fit parton distributions (fit 3 in [1]) contain a large gluonic content of the pomeron, with significant contributions at large fractional momenta. The results of this fit are superimposed on the data in figure 4 for the kinematic region over which the fit was performed.

The parton distributions extracted from the 1994 data have been evolved to the region $200 \leq Q^2 \leq 800$ GeV^2 for comparison with the new high Q^2 data. The results are presented in figure 3, with the contribution from the sub-leading exchange shown separately. Even in the large β region, which was not included in the fit, the QCD parameterisation gives a reasonable description of the data.

5.3 Two-gluon exchange model

In a recent paper [19], a parameterisation of the diffractive structure function in terms of three main contributions was proposed. In this model, the photon fluctuates to partonic states which scatter diffractively, the pomeron being modelled by the exchange of two gluons from the proton.

The first contribution $F_2^{D(3)}(q\bar{q}_T)$ corresponds to the diffractive scattering of the transverse $q\bar{q}$ component of the photon. The second, $F_2^{D(3)}(q\bar{q}g_T)$, corresponds to the transverse $q\bar{q}g$ component, and the third, $F_2^{D(3)}(q\bar{q}_L)$, which gives a higher twist contribution, corresponds to the longitudinal $q\bar{q}$ component. The three main contributions to $F_2^{D(3)}$ are then the following:

$$F_2^{D(3)}(q\bar{q}_T) = A\left(\frac{x_0}{x_{I\!P}}\right)^{n_2}\beta(1-\beta) \tag{9}$$

$$F_2^{D(3)}(q\bar{q}g_T) = B\left(\frac{x_0}{x_{I\!P}}\right)^{n_2}\alpha_S\left(\ln[\frac{Q^2}{Q_0^2}+1]\right)(1-\beta)^{\gamma} \tag{10}$$

$$F_2^{D(3)}(q\bar{q}_L) = C\left(\frac{x_0}{x_{I\!P}}\right)^{n_4}\left(\frac{Q_0^2}{Q^2}\right)\left(\ln[\frac{Q^2}{4Q_0^2\beta}+1.75]\right)^2\beta^3(1-2\beta)^2 \tag{11}$$

where

$$n_{2(4)} = n_{2(4)}^0 + n_{2(4)}^1 \ln\left[\ln\left(\frac{Q^2}{Q_0^2}\right)+1\right]. \tag{12}$$

The free parameters in the fit are the three normalisation factors A, B and C, the n_2^0, n_4^0, n_2^1 and n_4^1 factors which describe the $x_{I\!P}$ dependence of the cross section and are not predicted by QCD, and the γ parameter which describes the β dependence of the $q\bar{q}g$ term. An additional free parameter, x_0, was introduced to minimize any effect from n_2 and n_4 on the overall Q^2 shape. Q_0^2 is taken to be 1 GeV^2 and α_S is taken at the fixed value of 0.25. A sub-leading trajectory is added to the model as in equation (8). $F_2^{I\!R}$ is again constrained by [17], with an overall normalisation $n_{I\!R}$ and the value of $\alpha_{I\!R}$ as further free parameters.

n_2^0	1.198 ± 0.015 ± 0.041
n_2^1	0.104 ± 0.010 ± 0.041
n_4^0	1.395 ± 0.080 ± 0.005
n_4^1	0.000 ± 0.056 ± 0.001
γ	8.22 ± 0.78 ± 0.44
A	0.0184 ± 0.0040 ± 0.0022
B	0.0096 ± 0.0018 ± 0.0005
C	0.0108 ± 0.0067 ± 0.0003
x_0	0.992 ± 0.124 ± 0.050
$\alpha_{I\!R}$	0.664 ± 0.017 ± 0.063
$n_{I\!R}$	10.64 ± 1.04 ± 6.75
χ^2/dof	308.4 / 252

Table 1: Parameters obtained from the best fit solution to the two-gluon exchange model of Bartels et al. [19] . An additional sub-leading trajectory is added as explained in the text. The first and second errors on the parameters are respectively statistical and systematic. The χ^2 value is extracted with statistical errors only.

A fit is performed to the combined 1994 and low Q^2 1995 data with the restriction $Q^2 > 3$ GeV^2 to remain in the domain of perturbative QCD. Two χ^2 minima are found. The parameters for the better solution are given in table 1. The resulting value of γ is large. This leads to a strong β dependence of the $q\bar{q}g$ term, which is dominant only in the low β region. In this kinematic domain, contributions in which more than two partons emerge from the diffractive hard scattering have also been found to be important in measurements of hadronic final state observables in diffractive DIS [9, 20]. The longitudinal $q\bar{q}$ term is dominant for $\beta \gtrsim 0.75$ and low Q^2, indicating a strong higher twist contribution in this kinematic region. At intermediate β, the transverse $q\bar{q}$ term, varying as $\beta(1-\beta)$, is dominant. The second χ^2 minimum yields a value $\gamma = 0.14 \pm 0.07 \pm 0.05$, but is of significantly poorer quality ($\chi^2 = 335.1$ [$\sim 1.3/\mathrm{dof}$]) than the high γ solution. Both solutions to this model are shown compared to a subset of the low and intermediate Q^2 data in figure 5.

Using the parameters extracted from the fit of this model to the low and intermediate Q^2 data, the two solutions are compared to the new high Q^2 data in figure 6. The high γ solution, in which $q\bar{q}g$ contributions are restricted to low β, gives an acceptable description of the data, with some possible deviations at the largest β. The low γ solution, which has a larger higher twist contribution than the high γ solution, clearly fails to reproduce the Q^2 dependence at the highest β

5.4 BFKL based models of F_2^D

The 1994 and low Q^2 1995 measurements of $F_2^{D(3)}$ are also compared with two models in which the diffractive interaction is described by BFKL [21] dynamics. A QCD dipole model [22] is first investigated. Two different components are introduced [23]: a “quasi-elastic” term which represents the elastic scattering of a colour dipole arising from a $\gamma^* \to q\bar{q}$ fluctuation on the target proton and an “inelastic” term (triple-pomeron) which represents the sum of all dipole-dipole interactions and is dominant at large M_X. Once again, a sub-leading exchange is included as in equation (8) and only data points with $Q^2 > 3\ \mathrm{GeV}^2$ are considered. In this fit, $\chi^2/\mathrm{ndf} = 340.2/256$, evaluated with statistical errors only. The results are shown in Figure 4.

Finally, the model of Nikolaev et al. [24] is compared to the data. Diffractive dissociation is again modelled by a fluctuation of the photon into a $q\bar{q}$ or a $q\bar{q}g$ state, leading to a two-component structure function. The flux factors of the two components are different. This model differs from the others considered in that only the normalisation can be adjusted to the data and no sub-leading reggeon is included. The model is also shown in figure 5. The description is reasonable given that none of the parameters have been tuned to the data.

6 Conclusion

The diffractive structure function $F_2^{D(3)}$ has been measured in an extended kinematic domain at low and high Q^2. The qualitative features of these data are consistent with those of previous measurements at intermediate Q^2. Including all H1 published and preliminary data with $0.4 \leq Q^2 \leq 75~\mathrm{GeV}^2$ in a Regge phenomenological fit, the $x_{I\!P}$ dependence at fixed β and Q^2 can be described by the exchange of a pomeron and a sub-leading trajectory. The leading singularity is found to have an intercept larger than that describing soft hadronic interactions. An investigation of the scaling violations of $F_2^{D(3)}(x_{I\!P}, \beta, Q^2)$ at $x_{I\!P} = 0.005$ shows that for $\beta \lesssim 0.4$, the rise of F_2^D at fixed β previously observed persists in the low Q^2 regime. A NLO QCD fit to previously published H1 data, in which the pomeron has a gluon dominated structure, evolving according to the DGLAP evolution equations, gives a good description of the new data with $200 \leq Q^2 \leq 800~\mathrm{GeV}^2$. In a fit to the data of a two-gluon exchange model, higher twist contributions are found to be important at high β and low Q^2 . A reasonable description of the data can be obtained in models based on BFKL dynamics.

7 Acknowledgments

We are grateful to the HERA machine group whose outstanding efforts have made and continue to make this experiment possible. We thank the engineers and technicians for their work in constructing and now maintaining the H1 detector, our funding agencies for financial support, the DESY technical staff for continual assistance, and the DESY directorate for the hospitality which they extend to the non-DESY members of the collaboration. We thank Jochen Bartels and Robi Peschanski for fruitful discussions.

References

[1] H1 Collab., C.Adloff et al., Z. Phys. C76 (1997) 613.

[2] H1 Collab., I.Abt et al., Nucl. Instr. and Meth. A386 (1997) 310 and 348.

[3] H1 SPACAL group, R.D.Appuhn et al., Nucl. Instr. and Meth. A386 (1997) 397

[4] H1 Collab., C.Adloff et al., Nucl. Phys. B497 (1997) 3.

[5] H1 Collab., Technical Proposal for the Upgrade of the Backward Region of the H1 detector, DESY internal report PRC-93/02

[6] H1 Collab., "Luminosity Measurement in the H1 Experiment at HERA", contributed paper to the International Conference on High Energy Physics, Warsaw 1996, ICHEP96-pa17-026.

[7] U.Bassler, G.Bernardi, Nucl. Instr. and Meth. A361 (1995) 197.

[8] H1 Collab., C. Adloff et al., Z. Phys. C74 (1997) 221.

[9] H1 Collab., C.Adloff et al., Eur. Phys. J. C1 (1998) 495.

[10] H.Jung, Comp. Phys. Commun. 86 (1995) 147.

[11] L.Lönnblad, Comp.Phys.Commun. 71 (1992) 15.

[12] B.List, "Diffraktive J/Ψ-Produktion in Elektron-Proton-Stössen am Speicherring HERA", Diploma Thesis, Tech.Univ.Berlin, unpublished.

[13] G. Schuler, H. Spiesberger, Proceedings of the Workshop on "Physics at HERA", vol 3, eds. W. Buchmüller, G. Ingelman, DESY (1992) 317.

[14] R.Engel, Z.Phys.C66 (1995) 203., R.Engel, J.Ranft, Phys. Rev. D54 (1996) 4244.

[15] A.Kwiatkowski, H.Spiesberger, H.-J.Möhring, Comp. Phys. Commun. 69 (1992) 155.

[16] G. Ingelman, P. Schlein, Phys. Lett. B152 (1985) 256.

[17] M.Glück, E.Reya, A.Vogt, Z. Phys. C53 (1992) 651.

[18] G.Altarelli, G.Parisi, Nucl. Phys. B126 (1977) 298.
V.N.Gribov, L.N. Lipatov, Sov. J. Nucl. Phys. 15 (1972) 438 and 675.

[19] J.Bartels, J.Ellis, H.Kowalski, M.Wuesthoff, preprint DESY 98-034

[20] H1 Collab., C. Adloff et al., DESY 98-029, to appear in Phys. Lett. B.
H1 Collab., C. Adloff et al., DESY 98-044, to appear in Eur. Phys. J.
H1 Collab., paper 566 submitted to this conference.

[21] V.S.Fadin, E.A.Kuraev, L.N.Lipatov Phys. Lett. B60 (1975) 50.
I.I.Balitsky, L.N.Lipatov, Sov. J. Nucl. Phys. 28 (1978) 822.

[22] A.H.Mueller and B.Patel, Nucl. Phys. B425 (1994) 471.
A.H.Mueller, Nucl. Phys. B437 (1995) 107.
A.H.Mueller, Nucl. Phys. B415 (1994) 373.
H.Navelet, R.Peschanski, Ch.Royon, S.Wallon, Phys. Lett. B385 (1996) 357.

[23] A.Bialas, R.Peschanski, C.Royon, Phys. Rev. D57 (1998) 6899.
C.Royon, "Unified picture of DIS and diffractive DIS", Contributed paper to the DIS98 Workshop, Brussels, April 4-8 1998.

[24] M.Bertini et al., Phys. Lett. B422 (1998) 238
M.Genovese, N.N.Nikolaev, J. Exp. Theor. Phys. 81 (1995) 633.

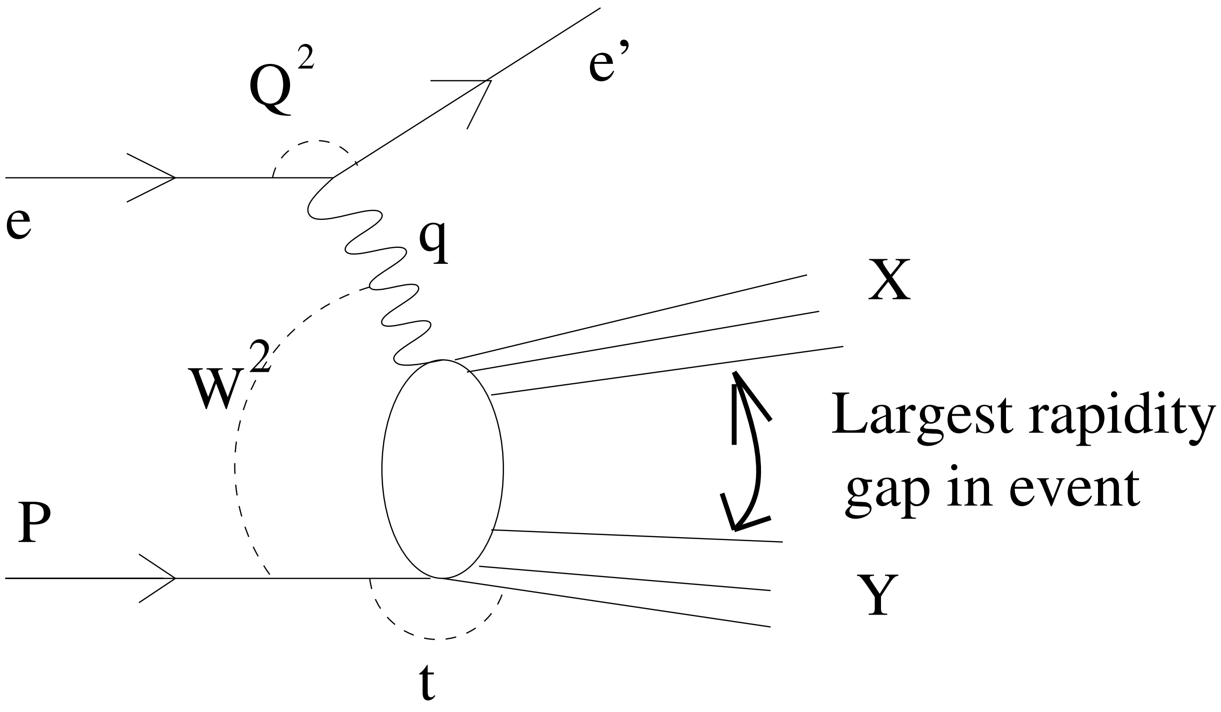

Figure 1: Illustration of the process $ep \to eXY$. The hadronic final state is composed of two distinct systems X and Y, which are separated by the largest interval in rapidity between final state hadrons.

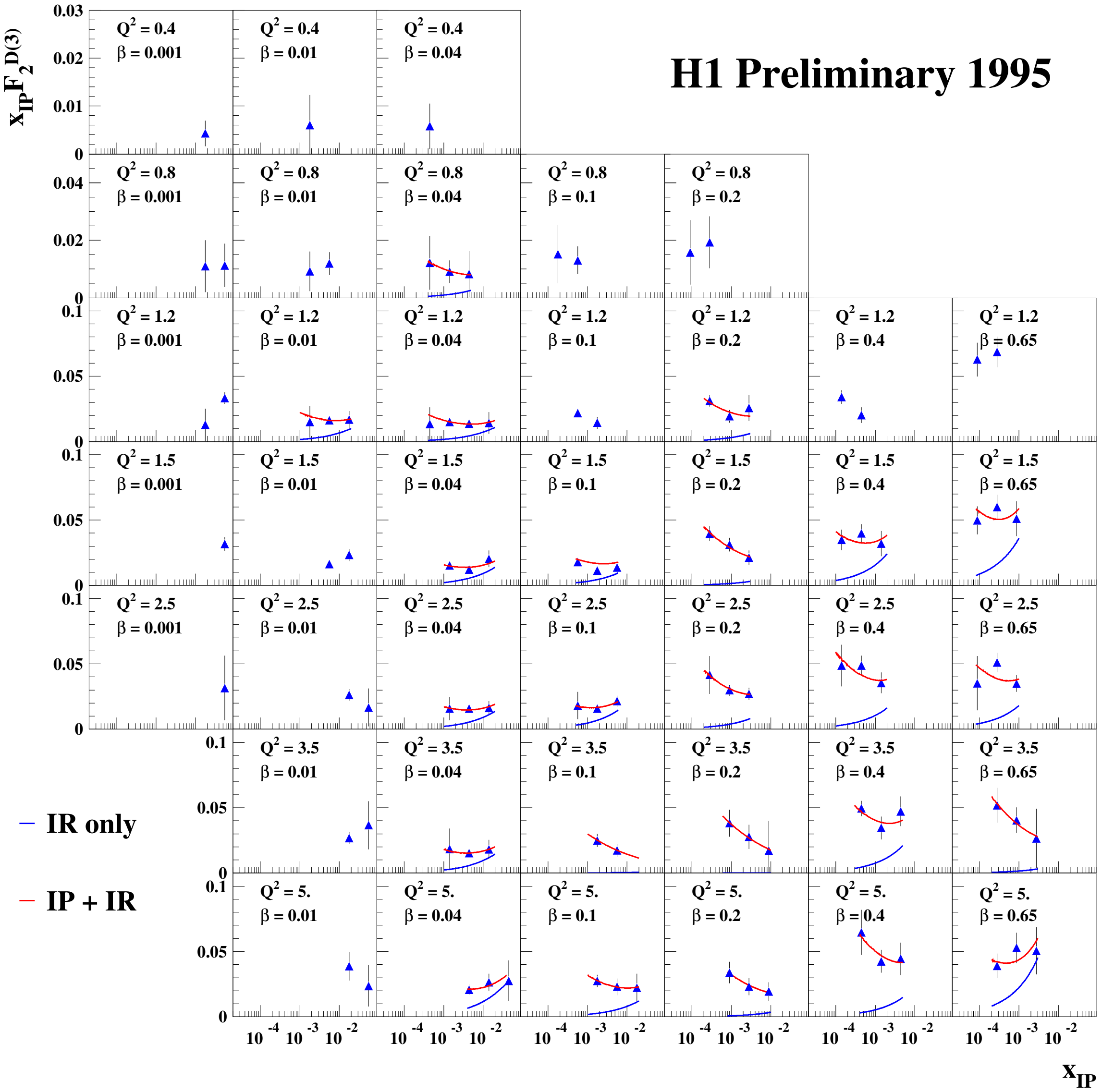

Figure 2: $x_{I\!P} \cdot F_2^{D(3)}$, shown as a function of $x_{I\!P}$ in bins of Q^2 and β. Statistical errors are shown added in quadrature with those systematic errors that vary between data points. An overall normalisation uncertainty of 4.0% is not shown. The data are compared with the results of a combined Regge phenomenological fit to 1994 and low Q^2 1995 H1 data with a diffractive ($I\!P$) and a sub-leading ($I\!R$) trajectory exchanged.

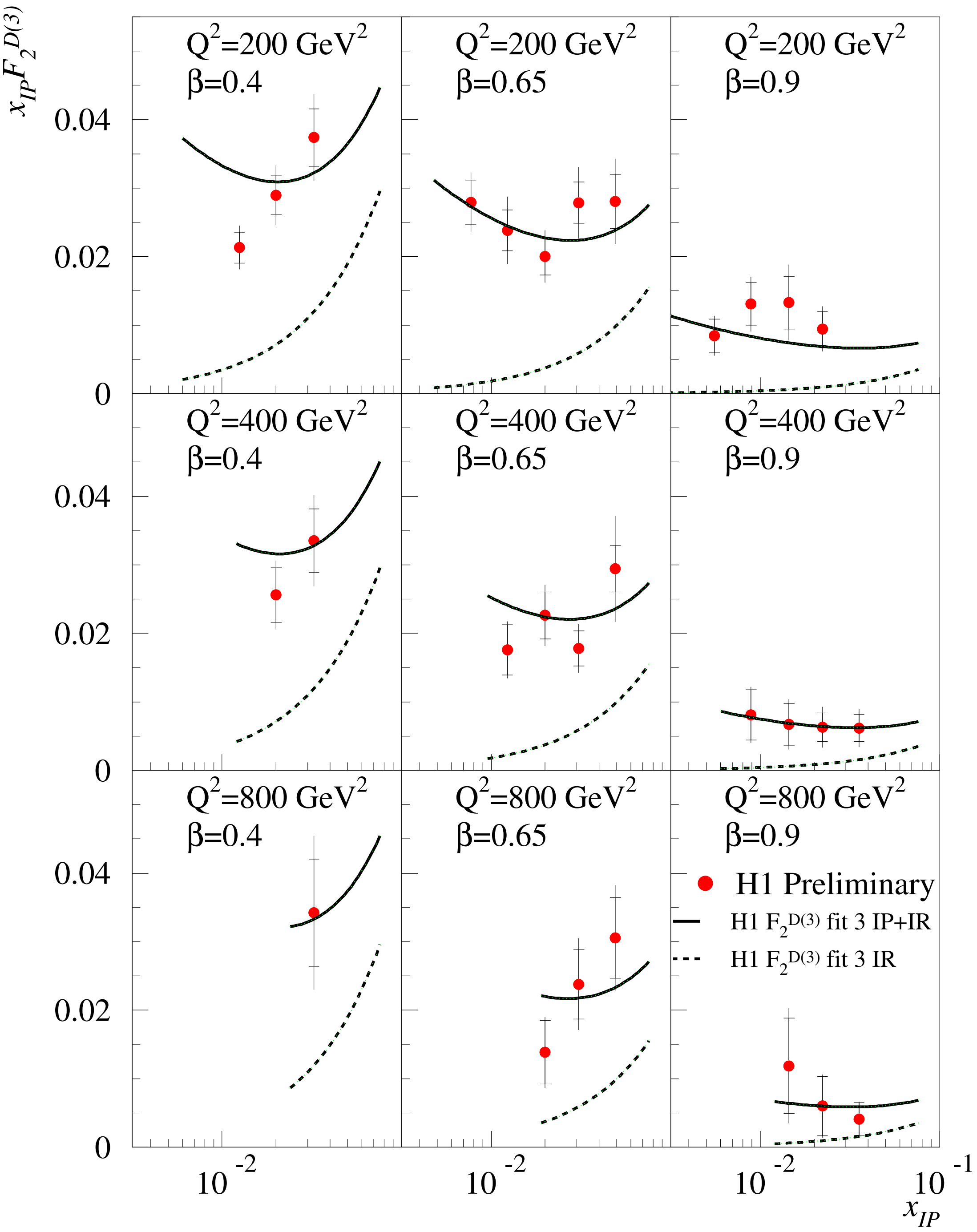

Figure 3: $x_{I\!P} \cdot F_2^{D(3)}$ for the large Q^2 measurement, shown as a function of $x_{I\!P}$ in bins of Q^2 and β. The inner errors bars show statistical errors only. The outer error bars show the statistical and systematic uncertainties added in quadrature. An overall normalisation uncertainty of 6.3% is not shown. The data are compared to a QCD fit to intermediate Q^2 data with parton distributions for the pomeron ($I\!P$) and sub-leading ($I\!R$) exchanges evolved into the large Q^2 region using the DGLAP equations.

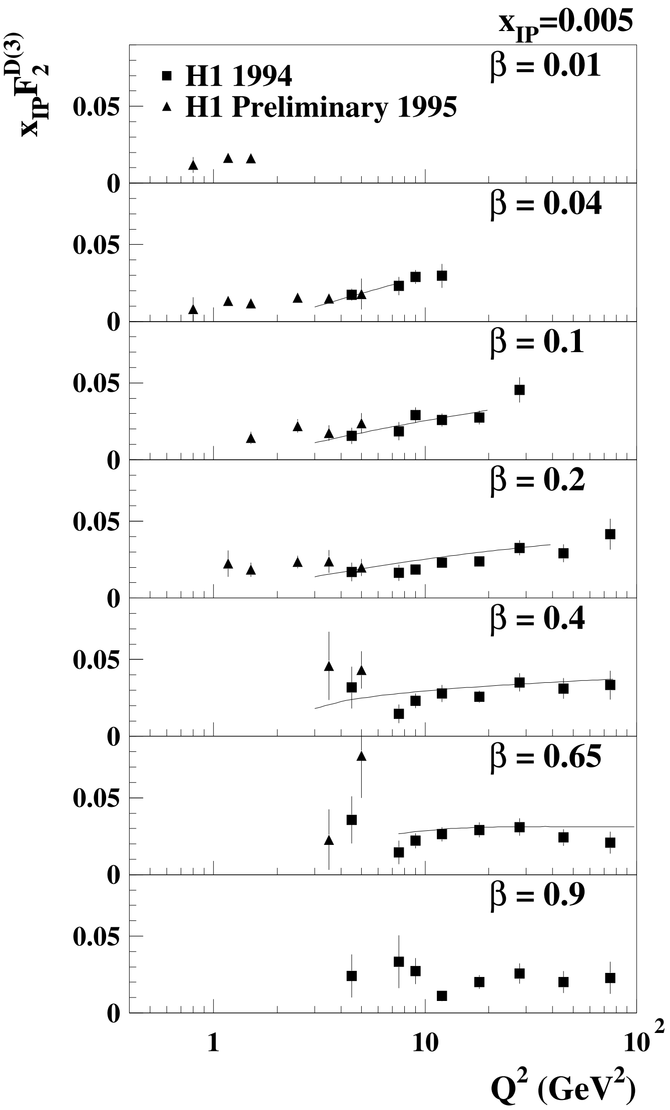

Figure 4: The structure function $x_{I\!P} \cdot F_2^{D(3)}$ ($x_{I\!P} = 0.005$), presented as a function of Q^2 in bins of β, over the full Q^2 range accessed with the 1994 and low Q^2 1995 data sets. The statistical errors are shown added in quadrature with those systematic errors that vary between data points. Overall normalisation uncertainties of 4.0% for the 1995 data and 6.3% for the 1994 data are not shown. The superimposed curves represent the result of the QCD fit to the 1994 data described in section 5.2 . This parameterisation is only shown in the kinematic region in which the fit was performed.

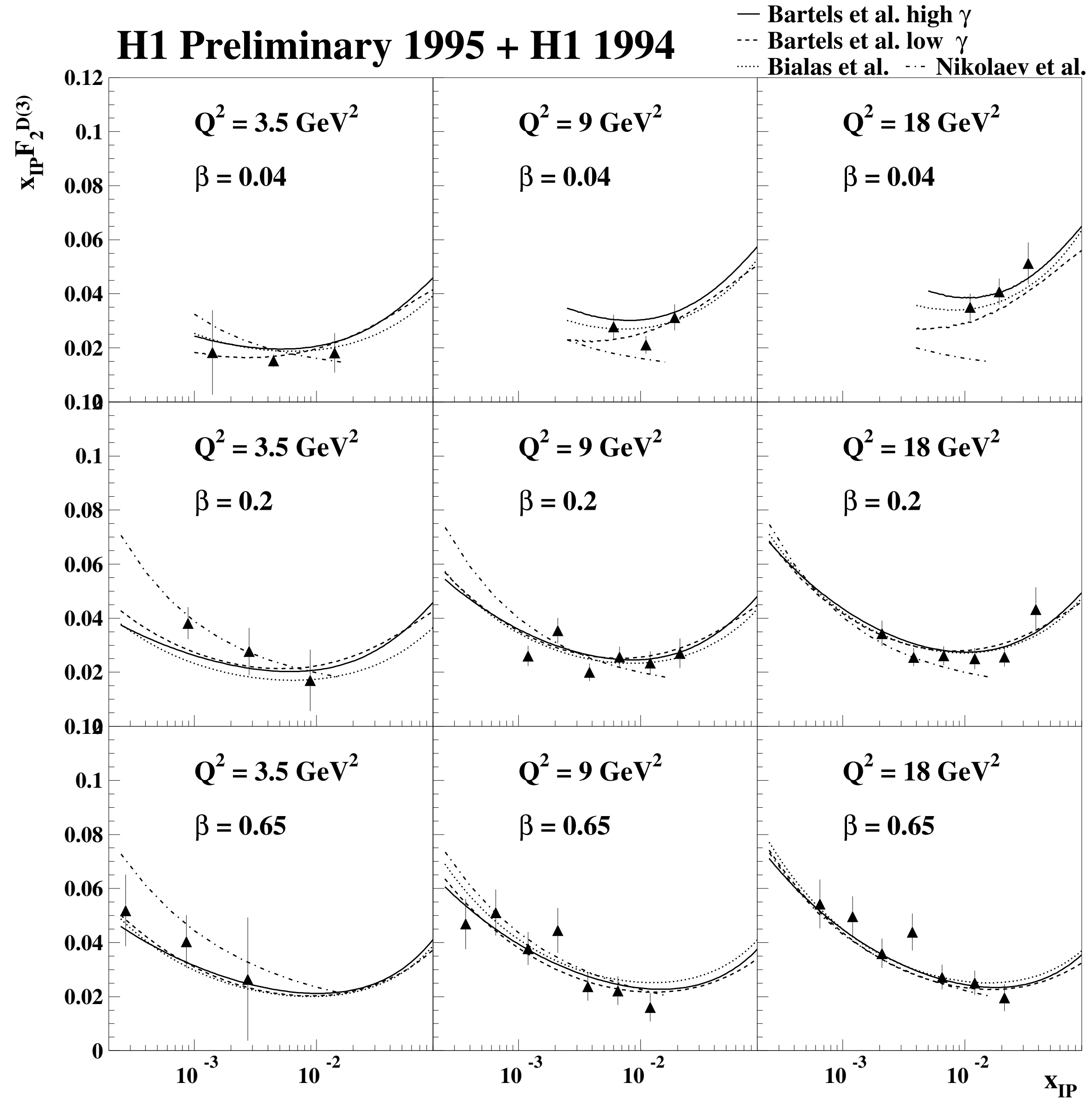

Figure 5: A subset of 1994 and low Q^2 1995 measurements of $x_{I\!P} F_2^{D(3)}$, showing the $x_{I\!P}$ dependence in bins of Q^2 and β. The statistical errors are shown added in quadrature with those systematic errors that vary between data points. Overall normalisation uncertainties of 4.0% for the 1995 data and 6.3% for the 1994 data are not shown. The data are compared to the results of a fit to the Bartels et al. two-gluon exchange model, to a fit based on the dipole model of Bialas et al. and to the prediction of the Nikolaev et al. model. For all models except that of Nikolaev et al., an additional sub-leading trajectory is added as described in the text.

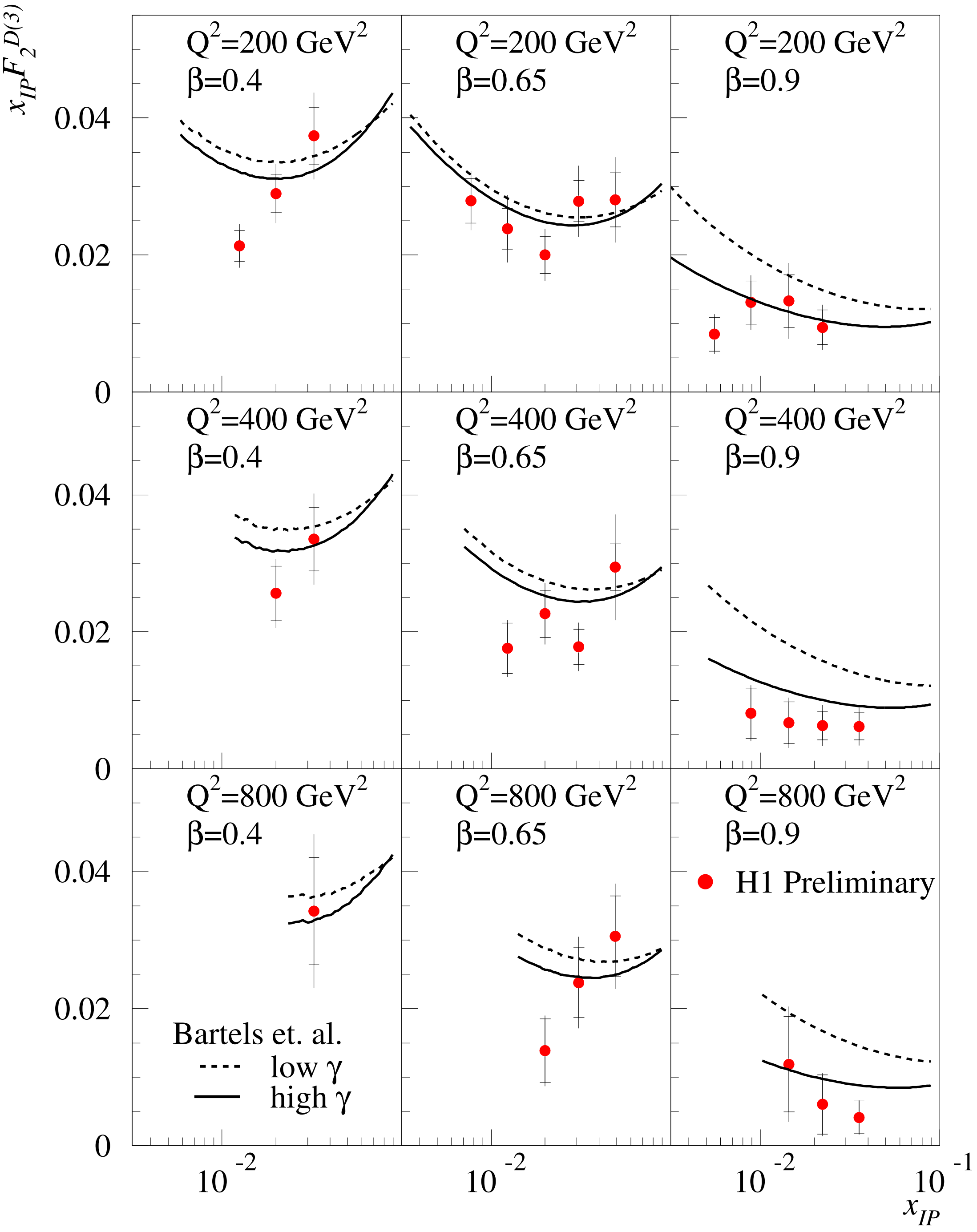

Figure 6: $x_{I\!P} \cdot F_2^{D(3)}$ for the large Q^2 measurement, shown as a function of $x_{I\!P}$ in bins of Q^2 and β. The inner errors bars show statistical errors only. The outer error bars show the statistical and systematic uncertainties added in quadrature. An overall normalisation uncertainty of 6.3% is not shown. The data are compared to the two solutions to the fit of the 2-gluon exchange parameterisation of Bartels et al., with an additional sub-leading trajectory added as described in the text.